HOKKAIDO UNIVERSITY

Title	Production cross sections of Mo, Nb and Zr radioisotopes from α -induced reaction on natZr
Author(s)	Murata, T; Aikawa, M; Saito, M; Ukon, N; Komori, Y; Haba, H; Takács, S
Citation	Applied Radiation and Isotopes, 144, 47-53 https://doi.org/10.1016/j.apradiso.2018.11.012
Issue Date	2019-02
Doc URL	http://hdl.handle.net/2115/79787
Rights	©2018. This manuscript version is made available under the CC-BY-NC-ND 4.0 license http://creativecommons.org/licenses/by-nc-nd/4.0/
Rights(URL)	http://creativecommons.org/licenses/by-nc-nd/4.0/
Type	article (author version)
File Information	Applied Radiation and Isotopes144_47-53.pdf

Instructions for use

Hokkaido University Collection of Scholarly and Academic Papers : HUSCAP

Production cross sections of Mo, Nb and Zr radioisotopes from α-induced reaction on ^{nat}Zr

T. Murata[a,*], M. Aikawa[b,c,†], M. Saito[c], N. Ukon[d], Y. Komori[e], H. Haba[e], S. Takács[f]

[a] School of Science, Hokkaido University, Sapporo 060-0810, Japan

[b] Faculty of Science, Hokkaido University, Sapporo 060-0810, Japan

[c] Graduate School of Biomedical Science and Engineering, Hokkaido University, Sapporo 060-8638, Japan

[d] Advanced Clinical Research Center, Fukushima Medical University, Fukushima City 960-1295, Japan

[e] Nishina Center for Accelerator-Based Science, RIKEN, Wako 351-0198, Japan

[f] Institute for Nuclear Research, Hungarian Academy of Sciences (ATOMKI), 4026 Debrecen, Hungary

Keyword

Molybdenum-99; Alpha particle irradiation; Zirconium target; Cross Section; Excitation function

Abstract

Cross sections of α-induced reactions on natural zirconium were measured up to 50 MeV using the stacked-foil technique, activation method and high resolution γ-ray spectrometry. The production cross sections of $^{93m,99}Mo$, $^{90g,92m,95g,95m,96}Nb$ and $^{88,89g,95}Zr$ were determined and compared with other experimental data measured earlier and result of theoretical calculations. The integral thick target yield of ^{99}Mo was deduced from the measured cross section data.

1. Introduction

There are several established and potential medical radioisotopes among Mo, Nb and Zr elements, such as ^{99}Mo, ^{93m}Mo (Sadeghi et al., 2010), ^{95g}Nb (Matthews and Molinaro, 1962), ^{90g}Nb (Milad and Mahdi, 2011) and ^{89g}Zr (see e.g. (Link et al., 2017) and references therein). Investigations on reactions to produce such radioisotopes are still insufficient and additional efforts are required (Capote et al., 2017). Based on known cross sections of the reactions, it is possible to select a better route for production of a

* Present address: Graduate School of Biomedical Science and Engineering, Hokkaido University, Sapporo

† Corresponding author: aikawa@sci.hokudai.ac.jp

radioisotope with less byproducts and with higher cost effectiveness.

The most important radioisotopes among them at present are the ^{99m}Tc and its parent isotope ^{99}Mo. Diagnosis using ^{99m}Tc ($T_{1/2}$ = 6.0067 h) covers about 80% of all nuclear medicine procedures worldwide (NEA, 2017). The radioisotope can be created by accelerators directly and also by the ^{99}Mo/^{99m}Tc generator technology. The production of ^{99}Mo ($T_{1/2}$ = 65.976 h) is currently relying on nuclear reactors (NEA, 2017; Van Noorden, 2013). However, most of the reactors are aged and alternative routes to produce the radioisotope currently attract much attention and are discussed (Van Noorden, 2013; Wolterbeek et al., 2014). One of the reactions to create ^{99}Mo is the ^{96}Zr(α,x)^{99}Mo reaction (Hagiwara et al., 2018; Pupillo et al., 2015, 2014). Three datasets of experimental cross sections measured earlier (Chowdhury et al., 1995; Hagiwara et al., 2018; Pupillo et al., 2014) were found. The three data sets, however, show quite different shapes from each other. In addition, the TENDL-2017 data, which compiles calculations of the TALYS code system (Koning and Rochman, 2012), are inconsistent with the experimental data. Therefore, we were motivated to perform experiments to measure the cross sections of the ^{96}Zr(α,x)^{99}Mo reaction.

Two independent irradiations using different targets and α-beam energies were performed. In the experiments, we could measure production cross sections of ^{93m,99}Mo, ^{90g,92m,95g,95m,96}Nb and ^{88,89g,95}Zr and deduce the integral yield of ^{99}Mo.

2. Experimental detail and data analysis

The stacked-foil technique, activation method and high resolution γ-ray spectrometry were used to determine cross sections. Two experiments using different targets and α-beam energies were performed at the AVF cyclotron of the RIKEN RI Beam Factory. The two stacked targets composed of 10×10 mm^2 natural Zr foils (99.2% purity) of different thicknesses (6.75 mg/cm^2, Goodfellow Co. Ltd., UK and 13.22 mg/cm^2, Nilaco Corp., Japan) and Ti foils for monitoring the beam parameters (99.6% purity, 2.43 mg/cm^2 and 2.40 mg/cm^2, Nilaco Corp., Japan). The isotopic composition of ^{nat}Zr is shown in Table 1 and used to convert cross sections of natural elements to ones of an isotopically pure case and vice versa. The thicknesses of the Zr and Ti foils were derived by measuring weights and sizes of original larger area foils before cutting them up. The composed stacked targets with Zr and Ti foils were irradiated with α-beams of two different energies, 29 and 50 MeV, respectively. The incident energies of the beams were determined by time-of-flight method using a plastic scintillator monitor (Watanabe et al., 2014). The energy degradation of the α-particles in the stacked targets was

calculated using the SRIM code (Ziegler et al., 2008). The irradiation with intensity of about 400 nA lasted for 2 hours in both cases. The intensity was measured by a Faraday cup. Correctness of the intensity and energy calculation inside the targets was assessed by the ^{nat}Ti(α,x)^{51}Cr monitor reaction. The γ-lines from the irradiated foils were measured by a HPGe detector (ORTEC GEM35P4-70) and analyzed by Gamma Studio (SEIKO EG&G). The detector calibrated by a multiple standard γ-ray point source consisting of ^{57,60}Co, ^{88}Y, ^{109}Cd, ^{113}Sn ^{137}Cs, ^{139}Ce and ^{241}Am was used. The reaction and decay data for the γ-ray spectrometry taken from NuDat 2.7 (National Nuclear Data Center, 2017) and QCalc (Pritychenko and Sonzogni, 2003) were summarized in Table 2.

The activation cross sections σ were deduced using the standard activation formula

$$\sigma = \frac{C_\gamma \lambda}{\varepsilon_d \varepsilon_\gamma \varepsilon_t N_t N_b (1 - e^{-\lambda t_b}) e^{-\lambda t_c} (1 - e^{-\lambda t_m})} \quad (1)$$

where C_γ is the measured net counts of the peak area, λ is the decay constant (s^{-1}), ε_d is the detector efficiency, ε_γ is the gamma-ray abundance, ε_t is the measurement dead time, N_t is the surface density of target atoms (cm^{-2}), N_b is the number of bombarding particles per unit time (s^{-1}), t_b is the bombarding time (s), t_c is the cooling time (s), and t_m is the acquisition time (s).

The cross sections of the ^{nat}Ti(α,x)^{51}Cr monitor reaction were derived and compared with the IAEA recommended values (Hermanne et al., 2018), which were an update to the IAEA-TECDOC-1211 values (Tárkányi et al., 2001), for assessment of beam parameters. The cross sections were derived from measurement of the 320.08-keV γ–ray (I_γ = 9.91%) from the ^{51}Cr decay ($T_{1/2}$ = 27.7025 d). The results in the two experiments are shown in Fig. 1. We could find almost good agreement with the recommended values (Hermanne et al., 2018) after the beam intensity was decreased by 6% and 8% for the 29 and 50 MeV cases, respectively. Adjustment of the beam energy was not required. Agreement with the recommended values indicates that the deduced beam intensity and the energy degradation calculation in the targets are correct and well reproduced.

3. Result and Discussion

The deduced production cross sections of ^{93m,99}Mo, ^{90g,92m,95g,95m,96}Nb and ^{88,89g,95}Zr isotopes are presented in Table 3 and 4 and are shown in Figs. 2-11 in comparison with experimental data studied earlier (Chowdhury et al., 1995; de la Vega Vedoya et al., 1981; Hagiwara et al., 2018; Pupillo et al., 2014) and the TENDL-2017 data (Koning and Rochman, 2012). The two sets of results using α-beam energies of 50 and 29 MeV

are described as #1 and #2 in the figures. They are consistent with each other at overlapping energy regions in all cases. The integral yield of ^{99}Mo was also derived from the measured cross sections of the 29 MeV case and shown in Fig. 12.

The total uncertainty of the measured cross sections was estimated to be 7.8-13.8% in most cases (50.6% at worst due to low net counts) and including statistical errors (0.3-10.8% in most cases and 49.8% at worst). It was estimated as the square root of the quadratic summation of the components; the beam intensity (5%), target thickness (1%), target purity (1%), γ intensity (<1%), detector efficiency (5%) and peak fitting (3%).

3.1 The ^{96}Zr(α,x)^{99}Mo reaction

The excitation function of the ^{96}Zr(α,x)^{99}Mo reaction was derived from measurements of the γ-line at 739.500 keV (I_γ = 12.20%). The spectra measured after cooling times of 48 hours (#1) and 91 hours (#2) were used. The half-lives of the parent nuclei of ^{99}Mo, ^{99g}Nb ($T_{1/2}$ = 15 s) and ^{99m}Nb ($T_{1/2}$ = 2.5 min), are very short and therefore only cumulative cross sections could be measured. Only reactions on ^{96}Zr in natural zirconium contributed to the ^{99}Mo production. The cross sections of the ^{96}Zr(α,x)^{99}Mo reaction were derived by taking into account the ^{96}Zr isotopic ratio in natural zirconium listed in Table 1. The results are shown in Fig. 2 with the experimental data of (Chowdhury et al., 1995; Hagiwara et al., 2018; Pupillo et al., 2014) and the TENDL-2017 data (Koning and Rochman, 2012). The data of the 29 MeV α-beam (#2) with statistical uncertainties better than those of the 50 MeV case (#1) are interpolated with the spline fitting up to 27.6 MeV. Our results show a smooth curve having a peak of 224.8 mb at around 14.6 MeV. The peak amplitude and position are very different from the two earlier experiments (Chowdhury et al., 1995; Pupillo et al., 2014), which have peaks of smaller amplitudes at higher energies. The peak of the TENDL-2017 data (Koning and Rochman, 2012) is smaller in amplitude and located at the lower energy side. On the contrary, our results are in complete agreement with the recent experimental data (Hagiwara et al., 2018).

3.2 The ^{nat}Zr(α,x)^{93m}Mo reaction

The cross sections for the ^{93m}Mo ($T_{1/2}$ = 6.85 h) production were derived from measurements of the 684.693-keV γ-line (I_γ = 99.9%) after cooling times longer than 16 hours. The excitation function of the ^{nat}Zr(α,x)^{93m}Mo reaction is shown in Fig. 3 in comparison with the experimental data (de la Vega Vedoya et al., 1981) and the TENDL-2017 data (Koning and Rochman, 2012). The present results are slightly larger

than the previous data above 34 MeV. However, the data show a large discrepancy below 30 MeV. The TENDL-2017 data are larger than ours between 22 and 38 MeV and above 45 MeV.

3.3 The $^{nat}Zr(\alpha,x)^{96}Nb$ reaction

Activity measurements selecting the 568.871-keV γ-line (I_γ = 58.0%) after cooling times longer than 48 hours were used for deducing the cross sections for the ^{96}Nb ($T_{1/2}$ = 23.35 h) production. The results are shown in Fig. 4 with the earlier experimental data of the literature (Chowdhury et al., 1995) and the TENDL-2017 data (Koning and Rochman, 2012). The earlier experimental data are in agreement with ours. The TENDL-2017 data underestimate the two experimental data.

3.4 The $^{nat}Zr(\alpha,x)^{95m}Nb$ reaction

The production cross sections of ^{95m}Nb ($T_{1/2}$ = 3.61 d) were derived from the γ-line at 235.690 keV (I_γ = 24.8%). The measurements were performed after cooling times longer than 48 hours. The measured net counts of the γ-line included the contribution from the decay of the parent ^{95}Zr ($T_{1/2}$ = 64.032 d). The contribution of ^{95}Zr was found to be less than 0.2% because of the long half-life of ^{95}Zr and small cross sections of the $^{nat}Zr(\alpha,x)^{95}Zr$ reaction (see section 3.8) and was neglected.

Our results are shown in Fig. 5 with the experimental data (Chowdhury et al., 1995) and the TENDL-2017 data (Koning and Rochman, 2012). The literature numerical data (Chowdhury et al., 1995) were published as isotopic cross sections of the $^{92}Zr(\alpha,x)^{95m}Nb$ reaction and therefore they were multiplied by the ^{92}Zr isotopic ratio in Table 1. The earlier experimental data and the TENDL-2017 data are lower than our results in the whole energy region up to 50 MeV.

3.5 The $^{nat}Zr(\alpha,x)^{95g}Nb$ reaction

The production cross sections of ^{95g}Nb ($T_{1/2}$ = 34.991 d) were derived from the γ-line at 765.803 keV (I_γ = 99.808%). We used the spectra recorded after cooling times longer than 48 hours similarly as the $^{nat}Zr(\alpha,x)^{95m}Nb$ reaction case. The net counts of the γ-line were affected by the decays of both ^{95}Zr and ^{95m}Nb. The contributions from decay of ^{95}Zr and ^{95m}Nb can be estimated knowing their cross sections (see section 3.4 and 3.8) and the corrected count rate can be obtained accordingly.

The results are shown in Fig. 6 with the experimental data (Chowdhury et al., 1995) and the TENDL-2017 data (Koning and Rochman, 2012). The isotopic numerical data of Chowdhury et al., 1995 were normalized by the ^{92}Zr isotopic ratio. Our results

are higher than the normalized data due to the contribution of the reactions on ^{94}Zr.

3.6 The ^{nat}Zr(α,x)^{92m}Nb reaction

The measurements of the 934.44 keV γ-line (I_γ = 99.15%) from the ^{92m}Nb decay ($T_{1/2}$ = 10.15 d) were performed after cooling times of 50 hours. The results are shown in Fig. 7 with the experimental data (Chowdhury et al., 1995) and the TENDL-2017 data (Koning and Rochman, 2012). The cross sections of the ^{90}Zr(α,x)^{92m}Nb reaction were listed in the literature (Chowdhury et al., 1995) and multiplied by the ^{90}Zr isotopic ratio in the figure. Our results are in good agreement with the TENDL-2017 data. The earlier experimental data (Chowdhury et al., 1995) are much larger than ours and the TENDL-2017 data.

3.7 The ^{nat}Zr(α,x)^{90g}Nb reaction

The excitation function of the ^{nat}Zr(α,x)^{90g}Nb reaction were derived from the measurement of the γ-line at 1129.224 keV (I_γ = 92.7%) from the ^{90g}Nb decay ($T_{1/2}$ = 14.60 h). The measurements were performed after a cooling time of minimum 67 hours. During the cooling time, ^{90}Mo ($T_{1/2}$ = 5.56 h) and ^{90m}Nb ($T_{1/2}$ = 18.81 s) were decayed to ^{90g}Nb. The derived cross sections are therefore cumulative ones.

The result is shown in Fig. 8 with earlier experimental data (de la Vega Vedoya et al., 1981) and TENDL-2017 data (Koning and Rochman, 2012). Our result is much smaller than the TENDL-2017 data in all energy regions. The earlier experimental data agree with our result below 46 MeV, however deviates above 46 MeV.

3.8 The ^{nat}Zr(α,x)^{95}Zr reaction

The excitation function of the ^{nat}Zr(α,x)^{95}Zr reaction was derived from measurements of the γ-line at 756.725 keV (I_γ = 54.38%). The cross sections were affected by the co-produced much shorter-lived ^{95}Y ($T_{1/2}$ = 10.3 min). We could obtain cumulative cross sections using the measurements after cooling times longer than 91 hours. The results are shown in Fig. 9 with the earlier experimental data (Chowdhury et al., 1995) and TENDL-2017 data (Koning and Rochman, 2012). Another experimental dataset (de la Vega Vedoya et al., 1981) was excluded because they are too large (larger than 13 mb) and are inconsistent with the others. Our results are in good agreement with the experimental data of the literature (Chowdhury et al., 1995) in the energy region where their data exist. The TENDL-2017 data shows quite different behavior.

3.9 The ^{nat}Zr(α,x)^{89g}Zr reaction

The production cross sections of ^{89g}Zr ($T_{1/2}$ = 78.41 h) were derived from the γ-line at 909.04 keV (I_γ = 99.04%) using measurements after cooling times longer than 48 hours. During the cooling times, three radioisotopes, ^{89g}Nb ($T_{1/2}$ = 2.03 h), ^{89m}Nb ($T_{1/2}$ = 66 min) and ^{89m}Zr ($T_{1/2}$ = 4.161 min) decayed completely to ^{89g}Zr.

The cumulative results are shown in Fig. 10 with experimental data of the literature (Yu and Blann, 1968) and TENDL-2017 data (Koning and Rochman, 2012). Our results are slightly lower than the earlier experimental data and the TENDL-2017 data below 40 MeV. Above 40 MeV, the TENDL-2017 data are lower than our result.

3.10 The ^{nat}Zr(α,x)^{88}Zr reaction

The production cross sections of ^{88}Zr ($T_{1/2}$ = 83.4 d) were derived from the γ-line at 392.87 keV (I_γ = 97.29%) using measurements after a cooling time of at least 67 hours. The result is shown in Fig. 11 with experimental data of the literature (Yu and Blann, 1968) and TENDL-2017 data (Koning and Rochman, 2012). The two experimental datasets are almost consistent with each other, however the TENDL-2017 data are slightly larger than the experimental data.

3.11 Integral yield of ^{99}Mo

The integral yield of ^{99}Mo from the ^{96}Zr(α,x)^{99}Mo reaction was deduced with the stopping powers S(E) obtained by the SRIM code (Ziegler et al., 2008) and the measured excitation function. End of bombardment activity (MBq/μA) (Otuka and Takács, 2015) for 1 hour irradiation up to 27.6 MeV is shown in Fig. 12 together with the other experimental data (Abe et al., 1984; Hagiwara et al., 2018; Pupillo et al., 2014). Our result is almost consistent with data of Abe et al., 1984 and Hagiwara et al., 2018, although larger than the one dataset (Pupillo et al., 2014).

4. Summary

The excitation functions for α-induced reactions on ^{nat}Zr to produce Mo, Nb and Zr isotopes were measured up to 50 MeV using the stacked foil technique, activation method and off-line γ-ray spectrometric technique. The production cross sections of ^{93m,99}Mo, ^{90g,92m,95g,95m,96}Nb and ^{88,89g,95}Zr were obtained. In accordance with a special attention to the ^{99}Mo production, the integral yield of ^{99}Mo produced from the ^{96}Zr(α,x)^{99}Mo reaction was deduced up to 27 MeV.

Acknowledgement

This work was carried out at RI Beam Factory operated by RIKEN Nishina Center and CNS, University of Tokyo, Japan. This work was supported by JSPS KAKENHI Grant Number 17K07004. The authors are grateful to Dr. M. Hagiwara (KEK) and Dr. H. Yashima (Kyoto University) for fruitful discussion and provision of experimental data.

Reference

Abe, K., Iizuka, A., Hasegawa, A., Morozumi, S., 1984. Induced radioactivity of component materials by 16-MeV protons and 30-MeV alpha particles. J. Nucl. Mater. 123, 972–976. https://doi.org/10.1016/0022-3115(84)90203-4

Capote, R., Nichols, A.L., Nortier, F.M., Carlson, B. V, Engle, J.W., Hermanne, A., Hussain, M., Ignatyuk, A. V, Kellett, M.A., Kibédi, T., Kim, G., Kondev, F.G., Lebeda, O., Luca, A., Naik, H., Nagai, Y., Spahn, I., Suryanarayana, S. V, Tárkányi, F.T., Verpelli, M., 2017. IAEA coordinated research project on nuclear data for charged-particle monitor reactions and medical isotope production. EPJ Web Conf. 146, 08007. https://doi.org/10.1051/epjconf/201714608007

Chowdhury, D.P., Pal, S., Saha, S.K., Gangadharan, S., 1995. Determination of cross section of α-induced nuclear reaction on natural Cr and Zr by stacked foil activation for thin layer activation analysis. Nucl. Instruments Methods Phys. Res. Sect. B 103, 261–266. https://doi.org/10.1016/0168-583X(95)00663-X

de la Vega Vedoya, M., Wasilevsky, C., Nassiff, S.J., 1981. Alpha particle induced reactions on zirconium. J. Radioanal. Chem. 67, 165–181. https://doi.org/10.1007/BF02516239

Hagiwara, M., Yashima, H., Sanami, T., Yonai, S., 2018. Measurement of the excitation function of ^{96}Zr(α,n)^{99}Mo for an alternative production source of medical radioisotopes. J. Radioanal. Nucl. Chem. https://doi.org/10.1007/s10967-018-6118-4

Hermanne, A., Ignatyuk, A. V., Capote, R., Carlson, B. V., Engle, J.W., Kellett, M.A., Kibédi, T., Kim, G., Kondev, F.G., Hussain, M., Lebeda, O., Luca, A., Nagai, Y., Naik, H., Nichols, A.L., Nortier, F.M., Suryanarayana, S. V., Takács, S., Tárkányi, F.T., Verpelli, M., 2018. Reference Cross Sections for Charged-particle Monitor Reactions. Nucl. Data Sheets 148, 338–382. https://doi.org/10.1016/j.nds.2018.02.009

Koning, A.J., Rochman, D., 2012. Modern Nuclear Data Evaluation with the TALYS Code System. Nucl. Data Sheets 113, 2841–2934. https://doi.org/10.1016/j.nds.2012.11.002

Link, J.M., Krohn, K.A., O'Hara, M.J., 2017. A simple thick target for production of ^{89}Zr using an 11 MeV cyclotron. Appl. Radiat. Isot. 122, 211–214.

https://doi.org/10.1016/j.apradiso.2017.01.037

Matthews, C.M.E., Molinaro, G., 1962. A study of the relative value of radioactive substances used for brain tumour localisation and of the mechanism of tumour: Brain concentration. Uptake in transplantable fibrosarcoma, brain and other organs in the rat. Br. J. Exp. Pathol. 44, 260–277.

Milad, E., Mahdi, S., 2011. Nuclear data for the cyclotron production of ^{117}Sb and ^{90}Nb. Chinese Phys. C 35, 248–254. https://doi.org/10.1088/1674-1137/35/3/007

National Nuclear Data Center, 2017. Nuclear structure and decay data on-line library, Nudat 2.7 [WWW Document]. URL http://www.nndc.bnl.gov/nudat2/

NEA, 2017. The Supply of Medical Radioisotopes: 2017 Medical Isotope Supply Review: ^{99}Mo/^{99m}Tc Market Demand and Production Capacity Projection 2017-2022, Nuclear Development NEA/SEN/HLGMR(2017)2. OECD, Paris.

Otuka, N., Takács, S., 2015. Definitions of radioisotope thick target yields. Radiochim. Acta 103, 1–6. https://doi.org/10.1515/ract-2013-2234

Pritychenko, B., Sonzogni, A., 2003. Q-value Calculator (QCalc) [WWW Document]. URL http://www.nndc.bnl.gov/qcalc/

Pupillo, G., Esposito, J., Gambaccini, M., Haddad, F., Michel, N., 2014. Experimental cross section evaluation for innovative ^{99}Mo production via the (α,n) reaction on ^{96}Zr target. J. Radioanal. Nucl. Chem. 302, 911–917. https://doi.org/10.1007/s10967-014-3321-9

Pupillo, G., Esposito, J., Haddad, F., Michel, N., Gambaccini, M., 2015. Accelerator-based production of ^{99}Mo: a comparison between the ^{100}Mo(p,x) and ^{96}Zr(α,n) reactions. J. Radioanal. Nucl. Chem. 305, 73–78. https://doi.org/10.1007/s10967-015-4091-8

Sadeghi, M., Enferadi, M., Nadi, H., Tenreiro, C., 2010. A novel method for the cyclotron production no-carrier-added ^{93m}Mo for nuclear medicine. J. Radioanal. Nucl. Chem. 286, 141–144. https://doi.org/10.1007/s10967-010-0622-5

Tárkányi, F., Takács, S., Gul, K., Hermanne, A., Mustafa, M.G., Nortier, M., Obložinský, P., Qaim, S.M., Scholten, B., Shubin, Y.N., Yousiang, Z., 2001. Beam monitor reactions, in: Charged Particle Cross-Section Database for Medical Radioisotope Production, IAEA-TECDOC-1211.

Van Noorden, R., 2013. Radioisotopes: The medical testing crisis. Nature 504, 202–204. https://doi.org/10.1038/504202a

Watanabe, T., Fujimaki, M., Fukunishi, N., Imao, H., Kamigaito, O., Kase, M., Komiyama, M., Sakamoto, N., Suda, K., Wakasugi, M., Yamada, K., 2014. BEAM ENERGY AND LONGITUDINAL BEAM PROFILE MEASUREMENT SYSTEM AT THE RIBF, in: Proceedings of the 5th International Particle Accelerator Conference (IPAC 2014). pp. 3566–3568.

Wolterbeek, B., Kloosterman, J.L., Lathouwers, D., Rohde, M., Winkelman, A., Frima, L., Wols, F., 2014. What is wise in the production of ^{99}Mo? A comparison of eight possible production routes. J. Radioanal. Nucl. Chem. 302, 773–779. https://doi.org/10.1007/s10967-014-3188-9

Yu, Y.-W., Blann, M., 1968. Excitation Functions, Recoil Ranges, and Statistical-Theory Analysis of Reactions Induced in Zr^{90} with 25- to 80-MeV Helium Ions. Phys. Rev. 170, 1131–1141. https://doi.org/10.1103/PhysRev.170.1131

Ziegler, J.F., Biersack, J.P., Ziegler, M.D., 2008. SRIM: the Stopping and Range of Ions in Matter [WWW Document]. https://doi.org/10.1016/j.nimb.2004.01.208.4

Figure captions

Fig. 1. Excitation function of the monitor $^{nat}Ti(\alpha,x)^{51}Cr$ reaction with the recommended values (Hermanne et al., 2018).

Fig. 2. The excitation function of the $^{96}Zr(\alpha,x)^{99}Mo$ reaction in comparison with literature values and the TENDL-2017 result.

Fig. 3. The excitation function of the $^{nat}Zr(\alpha,x)^{93m}Mo$ reaction in comparison with literature values and the TENDL-2017 result.

Fig. 4. The excitation function of the $^{nat}Zr(\alpha,x)^{96}Nb$ reaction in comparison with literature values and the TENDL-2017 result.

Fig. 5. The excitation function of the $^{nat}Zr(\alpha,x)^{95m}Nb$ reaction in comparison with literature values and the TENDL-2017 result.

Fig. 6. The excitation function of the $^{nat}Zr(\alpha,x)^{95g}Nb$ reaction in comparison with literature values and the TENDL-2017 result.

Fig. 7. The excitation function of the $^{nat}Zr(\alpha,x)^{92m}Nb$ reaction in comparison with literature values and the TENDL-2017 result.

Fig. 8. The excitation function of the $^{nat}Zr(\alpha,x)^{90g}Nb$ reaction in comparison with literature values and the TENDL-2017 result.

Fig. 9. The excitation function of the $^{nat}Zr(\alpha,x)^{95}Zr$ reaction in comparison with literature values and the TENDL-2017 result.

Fig. 10. The excitation function of the $^{nat}Zr(\alpha,x)^{89g}Zr$ reaction in comparison with literature values and the TENDL-2017 result.

Fig. 11. The excitation function of the $^{nat}Zr(\alpha,x)^{88}Zr$ reaction in comparison with literature values and the TENDL-2017 result.

Fig. 12. The activity of ^{99}Mo at the end of bombardment for 1 hour irradiation up to 27.6

MeV.

Tables

Table 1: Isotopic composition of natural zirconium

^{90}Zr	51.45%
^{91}Zr	11.22%
^{92}Zr	17.15%
^{94}Zr	17.38%
^{96}Zr	2.80%

Table 2: Reaction and decay data of reaction products

Nuclide	Half-life	Decay mode (%)	E_γ (keV)	I_γ (%)	Contributing reactions	Q-value (MeV)
^{99}Mo	65.976 h	β^- (100)	**739.500**	12.20	^{96}Zr(α,n)	-5.1
					^{96}Zr(α,p)^{99}Nb(β^-)	-8.0
^{93m}Mo	6.85 h	IT (99.88)	263.049	57.4(11)	^{94}Zr(α,5n)	-38.4
		β^- (0.12)	**684.693**	99.9(8)	^{92}Zr(α,3n)	-23.4
			1477.138	99.1(11)	^{91}Zr(α,2n)	-14.8
					^{90}Zr(α,n)	-7.6
^{96}Nb	23.35 h	β^- (100)	568.871	58.0(3)	^{96}Zr(α,tn)	-20.4
			778.224	96.45(22)	^{94}Zr(α,d)	-12.4
			1091.349	48.5(15)		
^{95g}Nb	34.991 d	β^- (100)	**765.803**	99.808(7)	^{96}Zr(α,t2n)	-27.3
					^{94}Zr(α,t)	-13.0
					^{92}Zr(α,p)	-6.5
					^{96}Zr(α,αn)^{95}Zr(ε)	-7.9
					^{94}Zr(α,^{3}He)^{95}Zr(ε)	-14.1
^{95m}Nb	3.61 d	IT (94.4)	**235.690**	24.8(8)		
		β^- (5.60)				
^{92m}Nb	10.15 d	ε+β^+ (100)	**934.44**	99.15	^{94}Zr(α,t3n)	-37.6
					^{92}Zr(α,tn)	-22.6
					^{91}Zr(α,t)	-14.0
					^{90}Zr(α,d)	-13.0
^{90g}Nb	14.60 h	ε+β^+ (100)	141.178	66.8(7)	^{92}Zr(α,t3n)	-42.5
			1129.224	92.7(5)	^{91}Zr(α,t2n)	-33.9
					^{90}Zr(α,tn)	-26.7
					^{91}Zr(α,5n)^{90}Mo(ε)	-45.7

					^{90}Zr(α,4n)^{90}Mo(ε)	-38.5
^{95}Zr	64.032 d	β^- (100)	724.192	44.27(22)	^{96}Zr(α,αn)	-7.9
			756.725	54.38(22)	^{94}Zr(α,^{3}He)	-14.1
					^{96}Zr(α,αp)^{95}Y(β^-)	-11.5
					^{94}Zr(α,3p)^{95}Y(β^-)	-25.5
^{89g}Zr	78.41 h	ε+β^+ (100)	**909.04**	99.04	^{94}Zr(α,α5n)	-42.8
					^{92}Zr(α,α3n)	-27.8
					^{91}Zr(α,α2n)	-19.2
					^{90}Zr(α,αn)	-12.0
					^{91}Zr(α,t3n)^{89}Nb(ε)	-44.0
					^{90}Zr(α,t2n)^{89}Nb(ε)	-36.8
^{88}Zr	83.4 d	ε (100)	**392.87**	97.29	^{92}Zr(α,α4n)	-37.1
					^{91}Zr(α,α3n)	-28.5
					^{90}Zr(α,α2n)	-21.3
					^{90}Zr(α,t3n)^{88}Nb(ε)	-49.3

Table 3. Measured cross sections by using 50 MeV α-beam

Energy (MeV)	$^{96}Zr(\alpha,x)^{99}Mo$ (mb)	$^{nat}Zr(\alpha,x)^{93m}Mo$ (mb)	$^{nat}Zr(\alpha,x)^{96}Nb$ (mb)	$^{nat}Zr(\alpha,x)^{95m}Nb$ (mb)	$^{nat}Zr(\alpha,x)^{95g}Nb$ (mb)	$^{nat}Zr(\alpha,x)^{92m}Nb$ (mb)	$^{nat}Zr(\alpha,x)^{90}Nb$ (mb)	$^{nat}Zr(\alpha,x)^{95}Zr$ (mb)	$^{nat}Zr(\alpha,x)^{89}Zr$ (mb)	$^{nat}Zr(\alpha,x)^{88}Zr$ (mb)
49.4 ±0.7		59.9 ±5.3	8.3 ±0.7	1.5 ±0.2	24.8 ±2.2	13.6 ±1.2	146.5 ±12.7	4.2 ±0.4	61.6 ±5.3	66.1 ±5.8
48.2 ±0.7		63.9 ±5.6	8.3 ±0.7	1.5 ±0.2	26.1 ±2.3	13.4 ±1.2	104.7 ±9.1	3.9 ±0.4	60.6 ±5.3	60.9 ±5.3
47.1 ±0.7		72.9 ±6.4	8.4 ±0.7	1.6 ±0.2	26.4 ±2.3	13.5 ±1.2	68.7 ±6.0	3.5 ±0.3	59.9 ±5.2	54.2 ±4.7
45.9 ±0.7		82.0 ±7.1	8.4 ±0.7	1.5 ±0.2	26.9 ±2.3	13.5 ±1.2	39.6 ±3.4	3.4 ±0.3	59.8 ±5.2	46.5 ±4.0
44.8 ±0.7		91.7 ±8.0	8.2 ±0.7	1.7 ±0.2	26.8 ±2.3	13.5 ±1.2	20.0 ±1.8	3.4 ±0.3	60.3 ±5.2	38.6 ±3.4
43.6 ±0.7		99.9 ±8.7	8.4 ±0.7	1.6 ±0.2	26.5 ±2.3	13.6 ±1.2	8.7 ±0.8	3.0 ±0.3	61.4 ±5.3	30.6 ±2.7
42.3 ±0.7		107.8 ±9.4	8.5 ±0.7	1.7 ±0.2	25.3 ±2.2	13.9 ±1.2	3.6 ±0.4	3.0 ±0.3	62.2 ±5.4	22.3 ±2.0
41.1 ±0.8		112.8 ±9.8	8.6 ±0.8	1.7 ±0.2	24.3 ±2.1	14.2 ±1.2	1.7 ±0.2	2.8 ±0.3	62.1 ±5.4	14.1 ±1.3
37.9 ±0.8		113.5 ±9.9	9.3 ±0.8	1.5 ±0.2	18.3 ±1.6	15.6 ±1.4	0.64 ±0.07	2.2 ±0.2	55.1 ±4.8	2.5 ±0.3
34.5 ±0.8	11.7 ±5.9	109.2 ±9.5	9.8 ±0.9	1.0 ±0.1	10.8 ±1.0	18.8 ±1.6		1.9 ±0.2	39.6 ±3.4	
30.9 ±0.9	24.9 ±6.0	82.2 ±7.2	8.8 ±0.8	0.70 ±0.09	5.8 ±0.5	22.4 ±1.9		1.5 ±0.2	22.3 ±1.9	
26.9 ±1.0	27.1 ±4.6	59.4 ±5.2	5.0 ±0.4	0.53 ±0.07	4.0 ±0.4	18.2 ±1.6		0.58 ±0.08	6.7 ±0.6	
22.5 ±1.1	45.4 ±4.8	67.4 ±5.9	1.03 ±0.09	0.55 ±0.06		5.0 ±0.4			0.29 ±0.03	
20.0 ±1.2	61.9 ±6.6	55.1 ±4.8	0.13 ±0.02	0.38 ±0.05		0.61 ±0.06			0.11 ±0.01	
17.4 ±1.4	142.5 ±13.4	17.1 ±1.5		0.19 ±0.03					0.13 ±0.01	
14.4 ±1.5	223.9 ±20.4	1.5 ±0.1		0.060 ±0.021					0.11 ±0.01	
10.9 ±1.8	46.4 ±4.2	0.009 ±0.002							0.11 ±0.01	
6.4 ±2.5									0.11 ±0.01	

Table 4. Measured cross sections by using 29 MeV α-beam

Energy (MeV)	$^{96}Zr(\alpha,x)^{99}Mo$ (mb)	$^{nat}Zr(\alpha,x)^{93m}Mo$ (mb)	$^{nat}Zr(\alpha,x)^{96}Nb$ (mb)	$^{nat}Zr(\alpha,x)^{95m}Nb$ (mb)	$^{nat}Zr(\alpha,x)^{95g}Nb$ (mb)	$^{nat}Zr(\alpha,x)^{92m}Nb$ (mb)	$^{nat}Zr(\alpha,x)^{95}Zr$ (mb)	$^{nat}Zr(\alpha,x)^{89}Zr$ (mb)
27.6 ±0.5	18.2 ±2.2		4.8 ±0.4	0.56 ±0.05	3.9 ±0.3	18.3 ±1.4	0.54 ±0.08	8.2 ±0.6
25.1 ±0.6	28.5 ±2.8		2.6 ±0.2	0.56 ±0.05	3.7 ±0.3	12.9 ±1.0	0.27 ±0.06	2.0 ±0.2
24.2 ±0.6	33.3 ±2.9	60.0 ±7.2	1.9 ±0.1	0.53 ±0.05	3.7 ±0.3	9.9 ±0.8		0.89 ±0.07
23.2 ±0.6	37.3 ±3.1	56.9 ±5.5	1.2 ±0.1	0.52 ±0.05	3.5 ±0.3	6.7 ±0.5		0.31 ±0.02
22.2 ±0.6	40.6 ±3.4	63.3 ±6.1	0.73 ±0.06	0.53 ±0.05	3.4 ±0.3	3.9 ±0.3		0.083 ±0.007
21.2 ±0.6	48.7 ±4.0	62.4 ±5.5	0.35 ±0.03	0.49 ±0.04	3.1 ±0.2	1.8 ±0.1		0.017 ±0.002
19.7 ±0.7	57.8 ±5.3			0.33 ±0.04	2.1 ±0.2	0.28 ±0.03		
18.1 ±0.7	92.3 ±7.5			0.24 ±0.02	1.2 ±0.1			
16.4 ±0.8	151.9 ±12.4			0.12 ±0.02	0.54 ±0.05			
14.6 ±0.8	224.8 ±18.3							
12.6 ±0.9	152.8 ±12.4							
10.4 ±1.0	13.9 ±1.2							

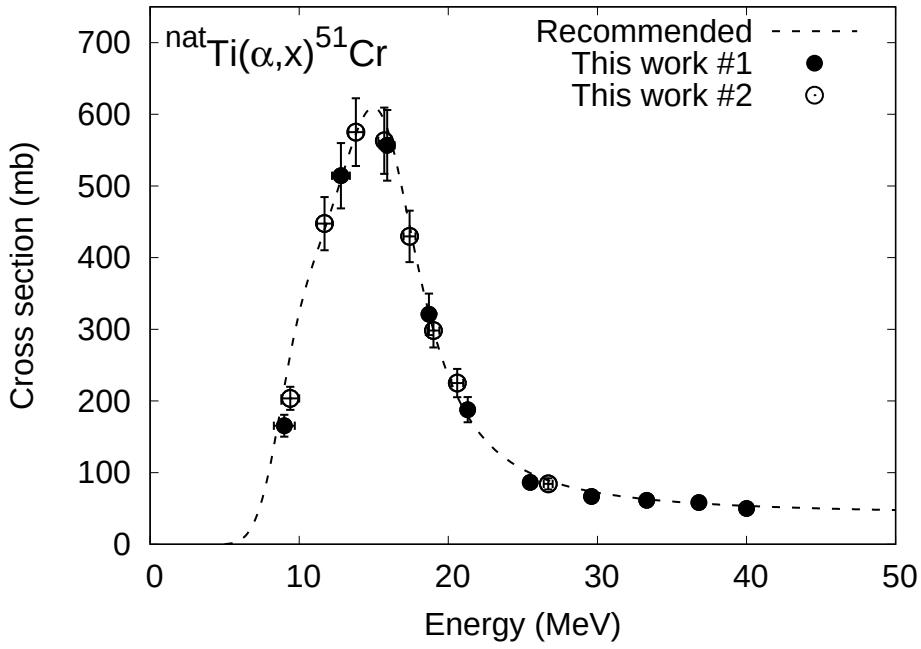
nat Ti(α,x) 51 Cr
Recommended
This work #1
This work #2
Cross section (mb)
Energy (MeV)
0
100
200
300
400
500
600
700
0
10
20
30
40
50

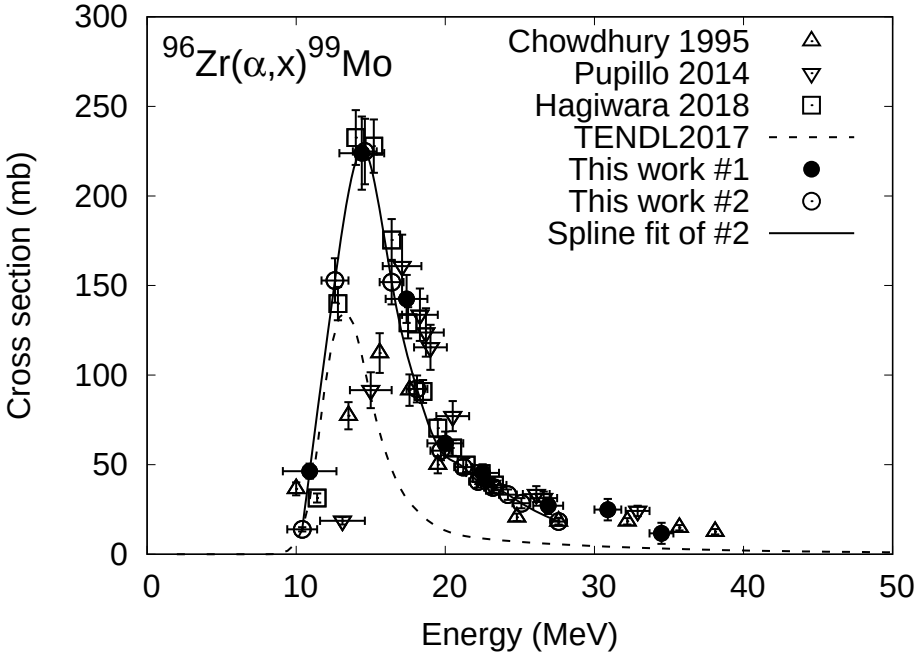
^{96}Zr(α,x)^{99}Mo
Chowdhury 1995
Pupillo 2014
Hagiwara 2018
TENDL2017
This work #1
This work #2
Spline fit of #2
Cross section (mb)
Energy (MeV)
0
50
100
150
200
250
300
0
10
20
30
40
50

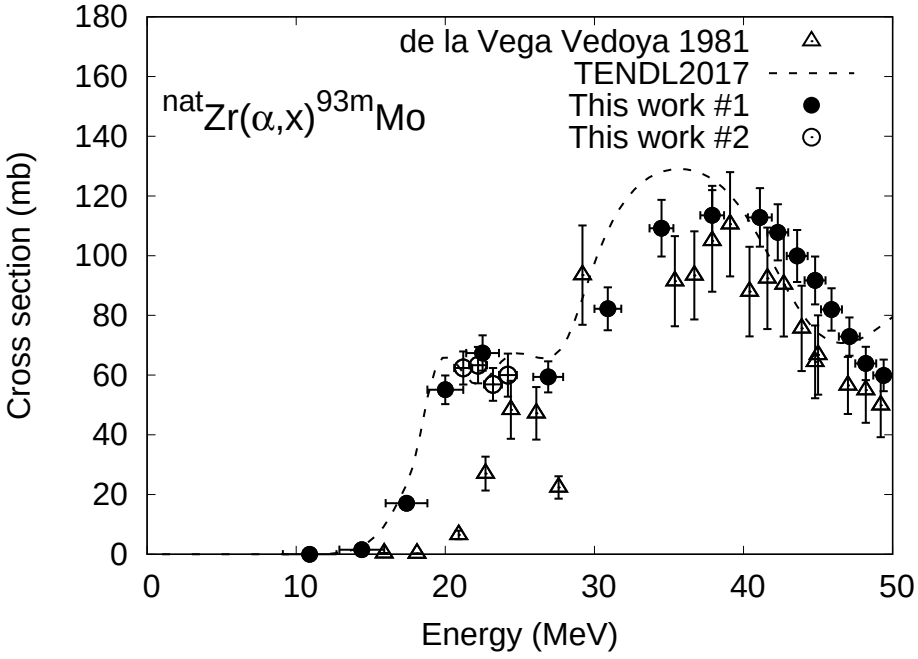
de la Vega Vedoya 1981
TENDL2017
This work #1
This work #2
natZr(α,x)93mMo
Cross section (mb)
Energy (MeV)
0
20
40
60
80
100
120
140
160
180
0
10
20
30
40
50

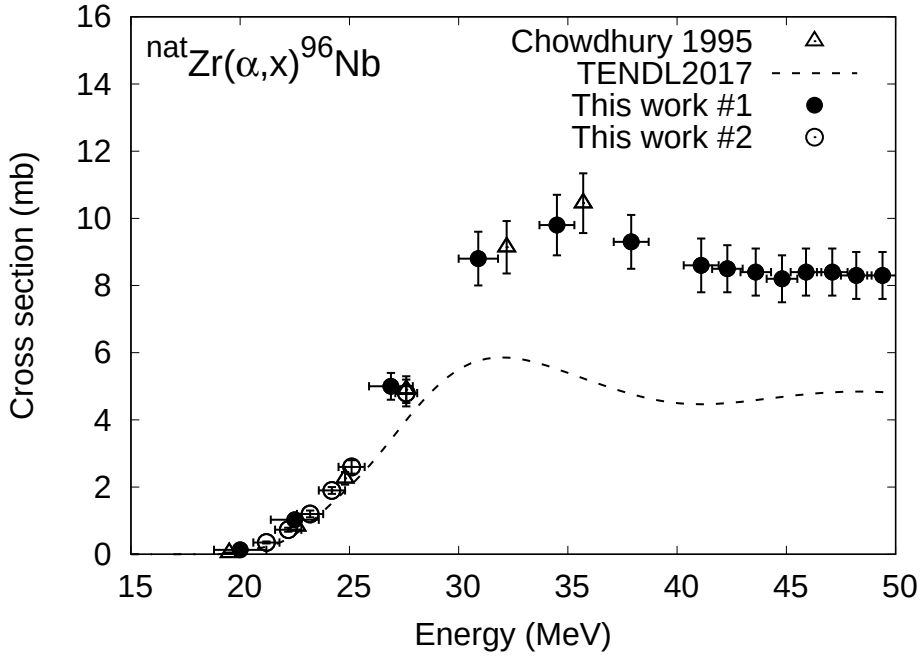
^{nat}Zr(α,x)^{96}Nb
Chowdhury 1995
TENDL2017
This work #1
This work #2
Cross section (mb)
Energy (MeV)
0
2
4
6
8
10
12
14
16
15
20
25
30
35
40
45
50

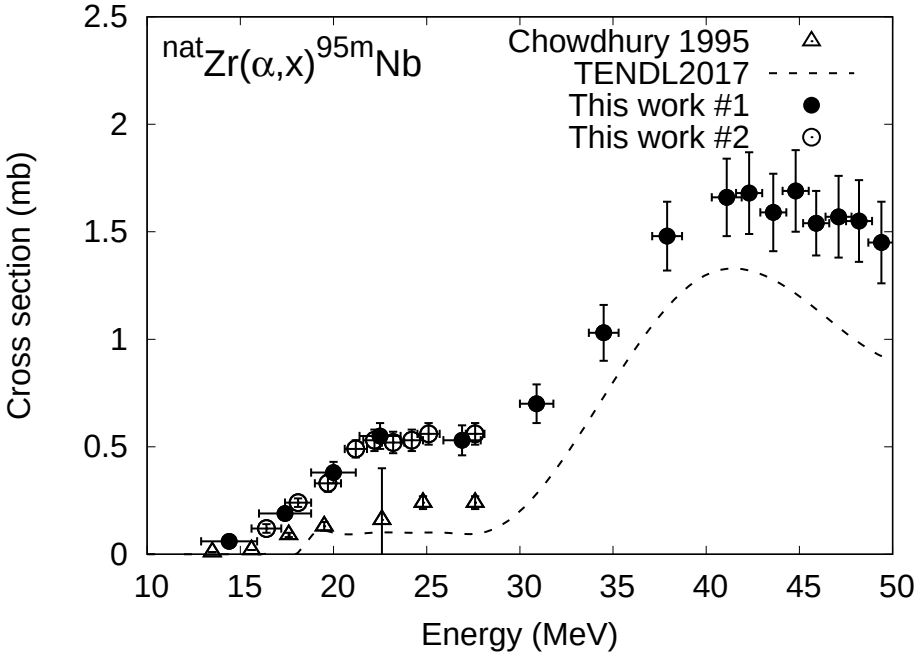
$^{nat}Zr(\alpha,x)^{95m}Nb$
Chowdhury 1995
TENDL2017
This work #1
This work #2
Cross section (mb)
Energy (MeV)
0
0.5
1
1.5
2
2.5
10
15
20
25
30
35
40
45
50

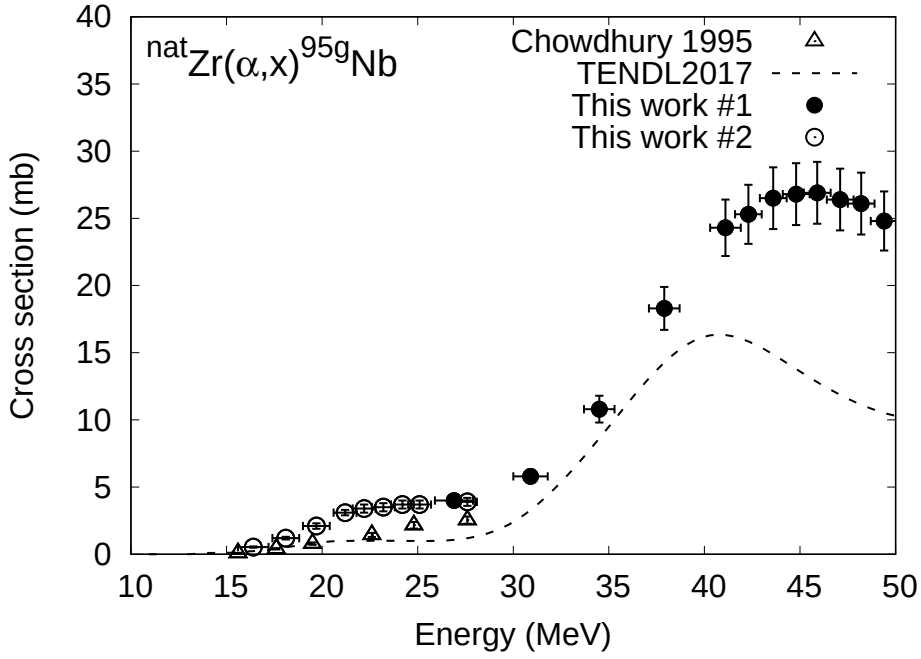
^{nat}Zr(α,x)^{95g}Nb
Chowdhury 1995
TENDL2017
This work #1
This work #2
Cross section (mb)
Energy (MeV)
0
5
10
15
20
25
30
35
40
10
15
20
25
30
35
40
45
50

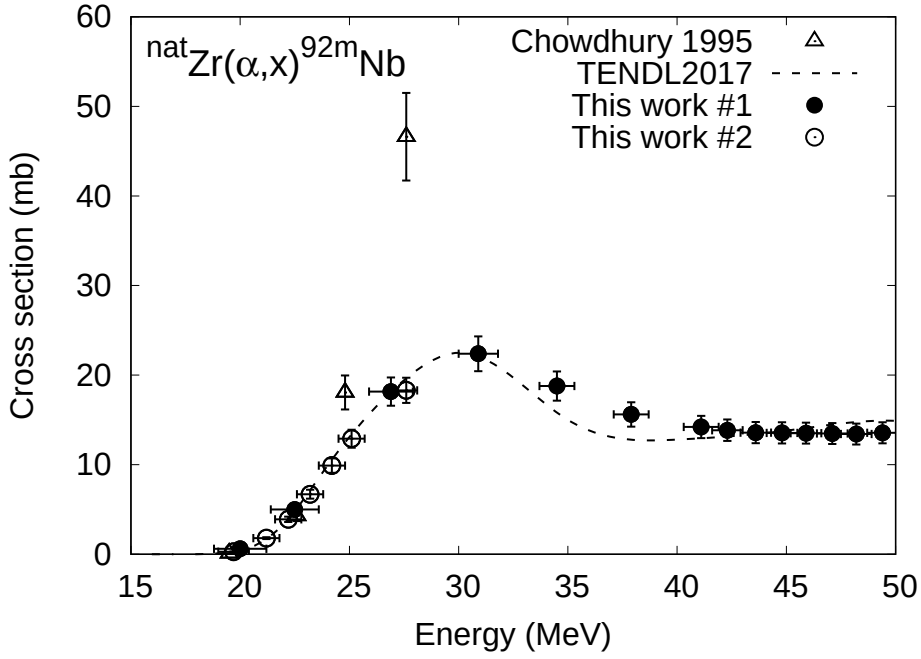
^{nat}Zr(α,x)^{92m}Nb
Chowdhury 1995
TENDL2017
This work #1
This work #2
Cross section (mb)
Energy (MeV)
0
10
20
30
40
50
60
15
20
25
30
35
40
45
50

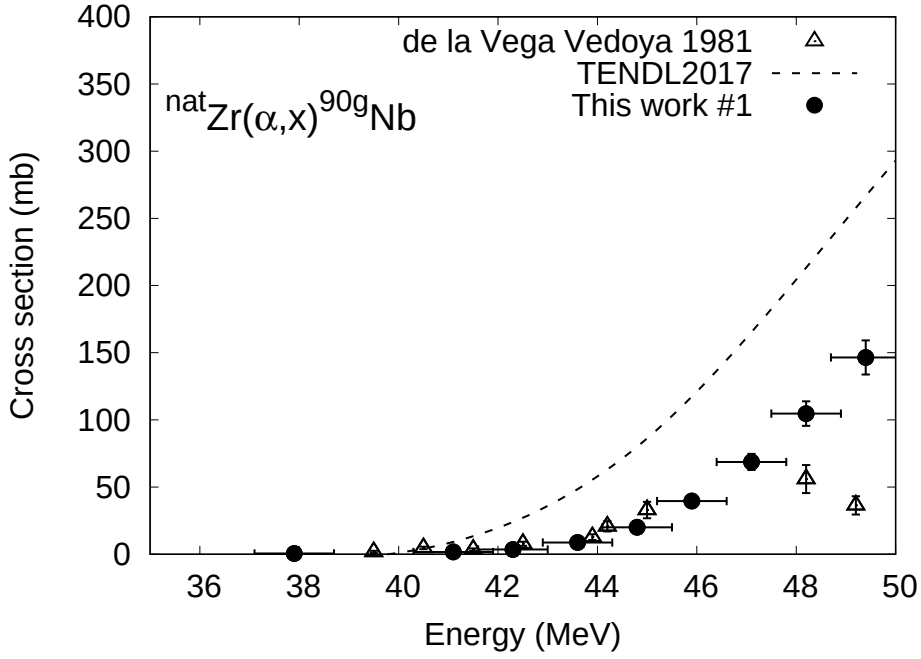
de la Vega Vedoya 1981
TENDL2017
This work #1
natZr(α,x)90gNb
Cross section (mb)
Energy (MeV)
0
50
100
150
200
250
300
350
400
36
38
40
42
44
46
48
50

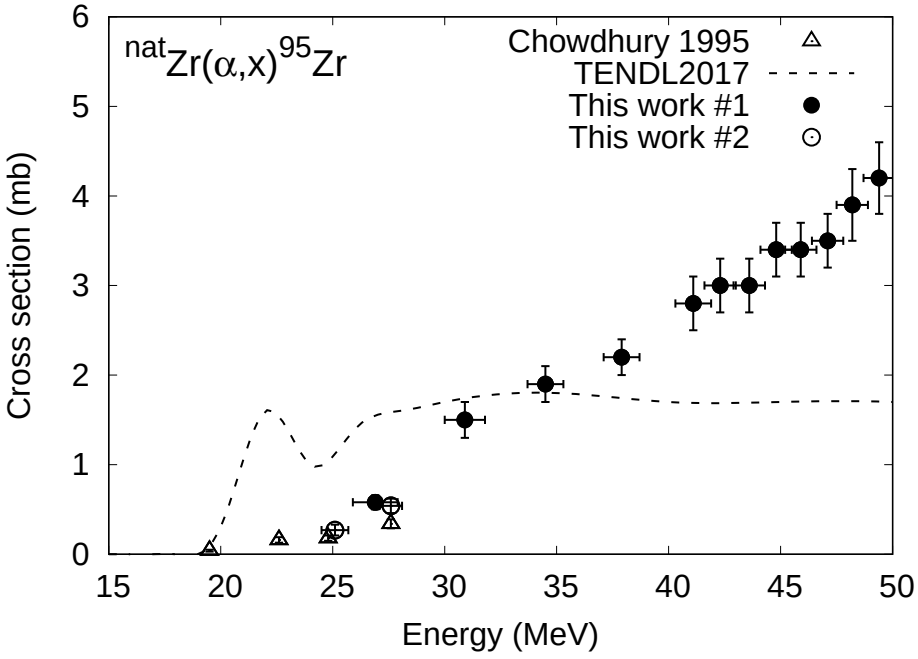
^{nat}Zr(α,x)^{95}Zr
Chowdhury 1995
TENDL2017
This work #1
This work #2
Cross section (mb)
Energy (MeV)
0
1
2
3
4
5
6
15
20
25
30
35
40
45
50

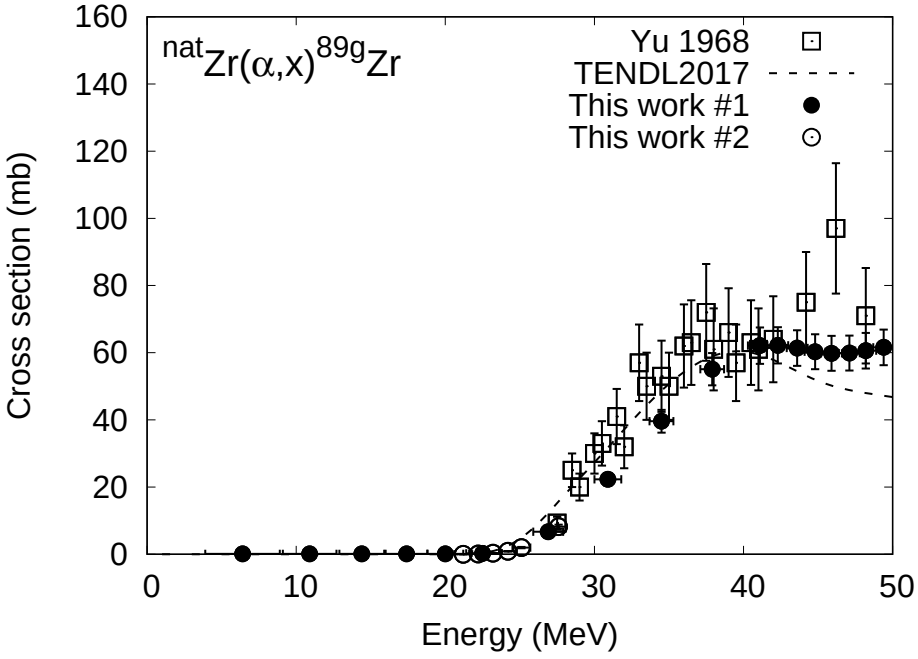
natZr(α,x)89gZr
Yu 1968
TENDL2017
This work #1
This work #2
Cross section (mb)
Energy (MeV)
0
20
40
60
80
100
120
140
160
0
10
20
30
40
50

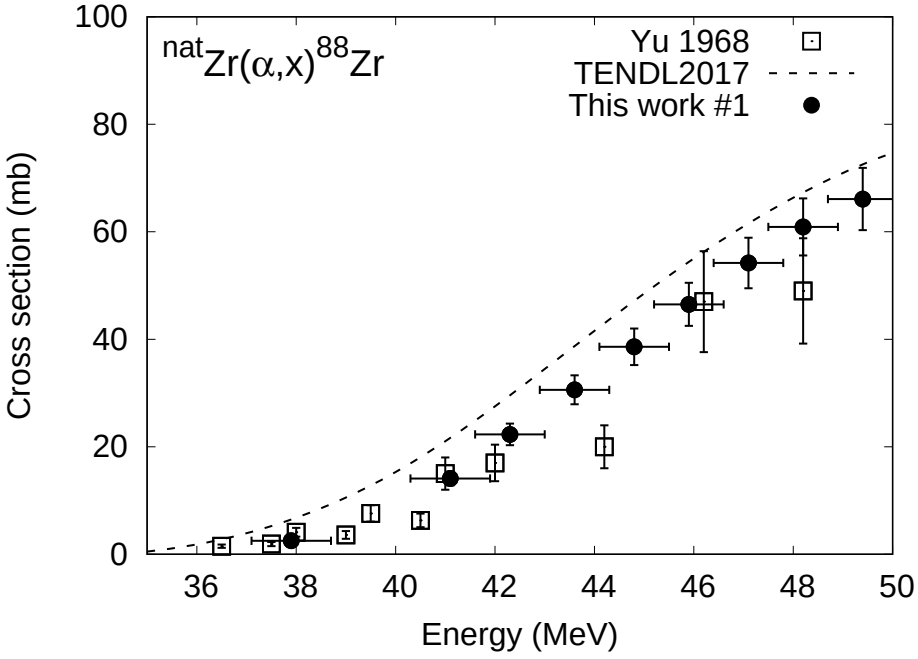
nat Zr(α,x)88 Zr
Yu 1968
TENDL2017
This work #1
Cross section (mb)
Energy (MeV)
0
20
40
60
80
100
36
38
40
42
44
46
48
50

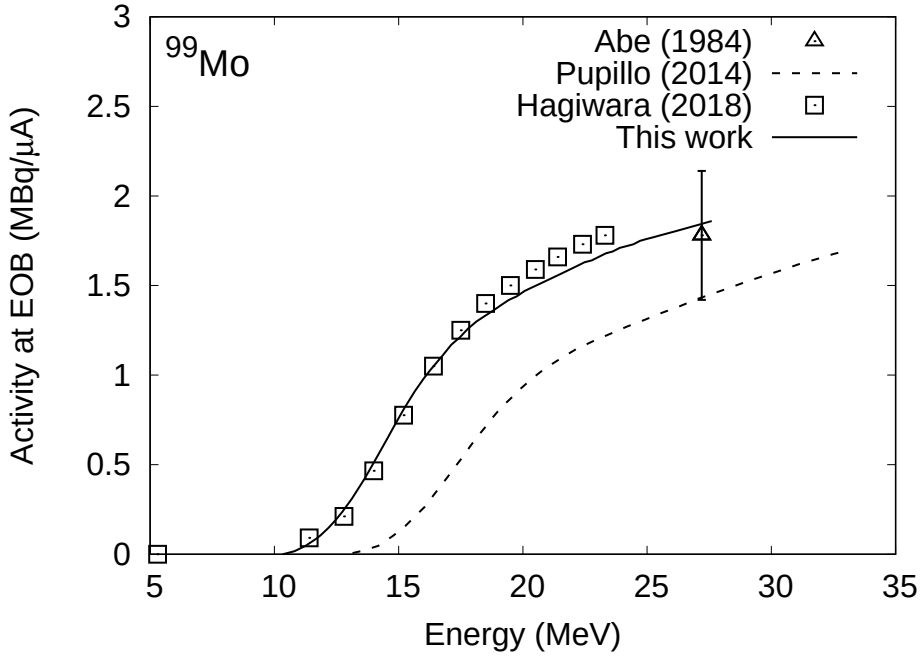
^{99}Mo
Abe (1984)
Pupillo (2014)
Hagiwara (2018)
This work
Activity at EOB (MBq/μA)
Energy (MeV)
0
0.5
1
1.5
2
2.5
3
5
10
15
20
25
30
35